A Flexible Method for Zoom Lens Calibration and Modeling Using a Planar Checkerboard

Bo Wu, Han Hu, Qing Zhu, and Yeting Zhang

Abstract

This paper presents a flexible method for zoom lens calibration and modeling using a planar checkerboard. The method includes the following four steps. First, the principal point of the zoom-lens camera is determined by a focus-of-expansion approach. Second, the influences of focus changes on the principal distance are modeled by a scale parameter. Third, checkerboard images taken at varying object distances with convergent image geometry are used for camera calibration. Finally, the variations of the calibration parameters with respect to the various zoom and focus settings are modeled using polynomials. Three different types of lens are examined in this study. Experimental analyses show that high precision calibration results can be expected from the developed approach. The relative measurement accuracy (accuracy normalized with object distance) using the calibrated zoom-lens camera model ranges from 1:5 000 to 1:25 000. The developed method is of significance to facilitate the use of zoom-lens camera systems in various applications such as robotic exploration, hazard monitoring, traffic monitoring, and security surveillance.

Introduction

One focus in the fields of close-range photogrammetry and computer vision research and applications is increasingly on zoom-lens cameras (Willson, 1994; Li and Lavest, 1996; Ahmed and Farag, 2000; Fraser and Al-Ajlouni, 2006; Ergun, 2010; Stamatopoulos and Fraser, 2011; Sanz-Ablanedo *et al.*, 2012). Zoom-lenses, due to their flexibility and controllability, have inherent advantages in the expansion of the imaging capabilities of fixed lens cameras (Willson, 1994; Li and Lavest, 1996). In the past, fixed lens cameras have been more commonly used for photogrammetric tasks than those with zoom lenses, mainly due to difficulties in metric modeling and calibration of zoom-lens cameras (Ahmed and Farag, 2000).

Bo Wu is with the Department of Land Surveying & Geo-Informatics, The Hong Kong Polytechnic University, Hung Hom, Kowloon, Hong Kong (bo.wu@polyu.edu.hk).

Han Hu is with the Department of Land Surveying & Geo-Informatics, The Hong Kong Polytechnic University, and the State Key Laboratory of Information Engineering in Surveying Mapping and Remote Sensing, Wuhan University, P.R. China.

Qing Zhu is with the Faculty of Geosciences and Environmental Engineering of Southwest Jiaotong University, Chengdu, P.R. China.

Yeting Zhang is with the State Key Laboratory of Information Engineering in Surveying Mapping and Remote Sensing, Wuhan University, P.R. China.

Camera calibration is the process of determining a camera's intrinsic parameters including principal distance, principal point offset, and lens distortions (Tsai, 1987). The principal distance and principal point offset are known as camera interior orientation (IO) parameters. They, together with the exterior orientation (EO) parameters, enable the derivation of 3D metric information in object space. Self-calibration approaches have been studied and used intensively in the photogrammetry community (Brown, 1971; Faig, 1975; Remondino and Fraser, 2006). This particular approach incorporates the intrinsic parameters of a camera into a photogrammetric bundle adjustment process so that all can be solved together and simultaneously with other unknowns. However, determinability of all parameters is not assured from self-calibration, which requires strong geometric configurations of the image networks for bundle adjustment to be achieved. In circumstances of applications using zoom-lens cameras such as 3D measurements and reconstruction of relatively long-range targets in areas not easily approachable to humans, monitoring of extremely hazardous situations such as mud-rock flows and landslides, automatic traffic monitoring and urban security surveillance, image networks with strong geometric configurations are difficult or sometimes impossible to obtain for all the lens settings. Therefore, zoom-lens camera calibration, as a stand-alone step, is preferred for these applications.

Previous zoom-lens calibration methods usually employ a special control field with precisely measured targets as ground truth. For example, Fraser and Al-Ajlouni (2006) employed a 3D control field for zoom-lens calibration comprised of a 140 object point array covering an area of approximately 5 m × 3 m. Ergun (2010) used a 3D calibration field to calibrate a zoom lens. The field contains 112 circular coded targets across different depth ranges. In close-range photogrammetric applications using zoom-lens cameras such as those mentioned above, the lens settings are subject to frequent changes, and accordingly, the zoom lens needs to be calibrated frequently to ensure ideal metric accuracies. However, frequent calibration of the in-use zoom-lens camera system in a specific control field is inconvenient or sometimes not feasible. In addition, calibration of zoom lens normally involves plenty of zoom and focus settings. Particularly, at large focused distance with zoom lens, the camera may need to be posed dozens of meters away from the calibration targets to capture sharp images. In this case, an in-door control field

may not be able to satisfy the calibration demand. Therefore, this paper proposes a strategy of using a more portable calibration target array, i.e., a planar checkerboard, for zoom lens calibration, which offers better flexibility and feasibility in real photogrammetric applications.

Most of the previous works on camera calibration generally either fix the focus at infinity or just use the autofocus function (Fraser and AL-Alouni, 2006) regardless of the variation to intrinsic parameters. However, both the increase of focal length and decrease of focused distance will lead to the decrease of depth of field (DOF), which will disturb the image acquisition and bring problems for camera calibration. For example, Figure 1 illustrates the changes of DOF with respect to the variations of focal length and focused distance. The problem of DOF decreases caused by focus changes becomes more serious when calibrating zoom lens with motorized zoom and focus settings, which has not been systematically studied in the past.

This paper presents a flexible method for zoom lens calibration considering focusing influences using a planar checkerboard. After presenting a literature review of previous research on camera calibration in the next section, a novel approach for zoom lens calibration is presented in detail in the third section. The performances of the approach are validated through experiments with pre-measured target arrays, and the results are presented in the fourth section, followed by Conclusions.

Related Work

Many studies on camera calibration have been reported. In the computer vision community, Tsai (1987) presented a seminal work for camera calibration. A camera model representing the parallel relationships between the distorted image points and the object points in a camera coordinate space was used. A least-squares optimization was adopted to solve the intrinsic and extrinsic parameters of the camera. In Tsai's method, only one image of a 3D or coplanar grid pattern with more

than eight control points is needed for the camera calibration. However, Tsai's method only takes account for the radial distortions of the camera. In the widely cited work of Zhang (2000), a pinhole model is used to represent the transformation from 2D image to 3D object space. Image distortions are taken into consideration using maximum likelihood estimation. Two or more images of coplanar grid pattern with different orientations are needed for the camera calibration. The homographic matrix between the image points and object points is exploited to solve the camera parameters, followed by a linear minimization of image projection errors with Levenberg-Marquardt algorithm (Zhang, 2000).

In the photogrammetry community, the self-calibration approaches, indicated above, have been widely used from 1970s (Brown, 1971; Faig, 1975). The no requirement of object space control for the self-calibration technique made it an effective means of camera calibration. The non-linear collinear equations or other models with additional parameters (camera intrinsic parameters) used in bundle adjustment to model the perspective transformation from 2D images to 3D object space has changed little since the 1970s. Many combinations of additional parameters have been evaluated (Abraham and Hau, 1997). However, the new observations introduced by additional parameters and the correlations among or between those parameters and the exterior orientation parameters can degrade the normal equation system, hence affecting their solutions. With this in mind, a more reasonable approach is the employment of only those additional parameters which have prominent physical justifications such as lens distortions. The cubic term in the radial distortion model, known as K_1, has been proved to be sufficient for most non-metric 35 mm and 70 mm camera lenses and C-mount lenses utilized by video cameras (Fryer and Brown, 1986). Several strict constraints for a satisfactory self-calibration have been given previous (Fraser, 1997; Clarke and Fryer, 1998; Remondino and Fraser, 2006). They are (a) overlap of at least three images under a fixed camera setting, (b) stability of camera internal parameters and targets in object space, (c) an ample convergent angle for better depth accuracy, and (d) well distributed targets from a diversity of camera locations. However, these criteria limit the use of self-calibration approaches for zoom-lens calibration.

Various variable-parameter camera models and calibration methods have been reported for zoom-lens calibration (Willson, 1994; Tarabanis *et al.*, 1994; Wiley and Wong, 1995; Li and Lavest, 1996; Shih *et al.*, 1996; Ahmed and Farag, 2000; Fraser and Al-Ajlouni, 2006). In the widely cited work of Willson (1994), a camera with automated zoom lenses was calibrated across continuous ranges of focus and zoom to produce an adjustable perspective-projection camera model. The Camera's intrinsic parameters were independently derived using the method of Tsai (1987) for images taken at various settings of zoom and focus. Low order bivariate polynomials were made fit for the camera's intrinsic parameters. Global optimization of all the calibration data was employed to optimize the coefficients of the fitted polynomials. Currently, more off-the-shelf cameras with zoom-lenses are available on the market thus better enabling recent research to focus on medium-accuracy photogrammetric measurements using such consumer-grade cameras. A representative work has been reported by Fraser and Al-Ajlouni (2006). This work presented a zoom-dependent calibration method, in which the camera's intrinsic parameters were expressed as simple functions of the focal length. Experimental results using four different cameras rendering almost all photos infinity focused show that the proportional accuracy (accuracy normalized with object size) in 3D object point determination ranges from 1:9 000 to 1:40 000.
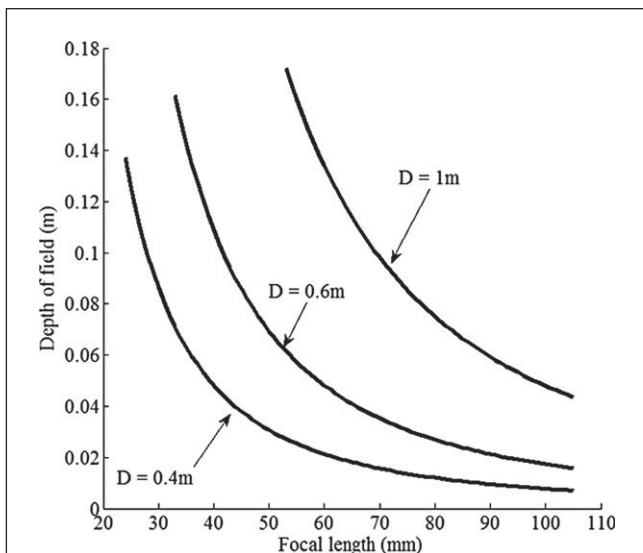

Figure 1. Decrease in depth of field (DOF) with increasing focal lengths at three different focused distances (1 m, 0.6 m, and 0.4 m). The standard values of f-number (relative aperture) and circle of confusion are used in the calculation of DOF.

One common feature shared by previous research on zoom-lens calibration is the intention to empirically model camera intrinsic parameter variations with changing zoom and/or focus settings, using special 3D calibration fields. Compared with previous work, this study highlights the following three aspects: (a) the development of a flexible method for zoom-lens calibration and modeling using a planar checkerboard, (b) the investigation of influence of focus to the intrinsic parameters which cannot be ignored especially in near focused distance, and (c) the development of a strategy using a scale parameter to compensate for the influences of focus changes on the principal distance which enables autofocus in zoom lens calibration process. The details of this approach are specifically discussed below.

Zoom-Lens Calibration and Modeling Using a Checkerboard

There are various types of zoom lens systems. The most complex ones may have tens of lens elements and assemble multiple moving components. But most of the zoom lens systems follow a basic two-step scheme in arranging the lens assembly of two separate parts (Malacara and Malacara, 1994): (a) A zoom system which alters the size of a beam of light travelling through it, thus the overall zoom setting of the lens system, and (b) A focusing system, similar to the standard prime lens, controls the focused distance (i.e., focus setting). Figure 2 illustrates the operational procedure of a simple zoom lens camera with a zoom system and a focusing lens. In Figure 2, the size of the parallel light beam is changing while moving the negative lens L_2 in the zoom system. The maximum zoom setting corresponds to the maximum light beam size and vice versa.

It is explicitly indicated in Figure 2 that the principal distance is monotonic with varying zoom/focus settings. The principal point, when lens elements are aligned perfectly along the axial direction, should meet with the center of the image format. However, in practice it may stray from the exact image center due to the complexity of lens assembling and the integration of gears or servos for controlling lens movement.
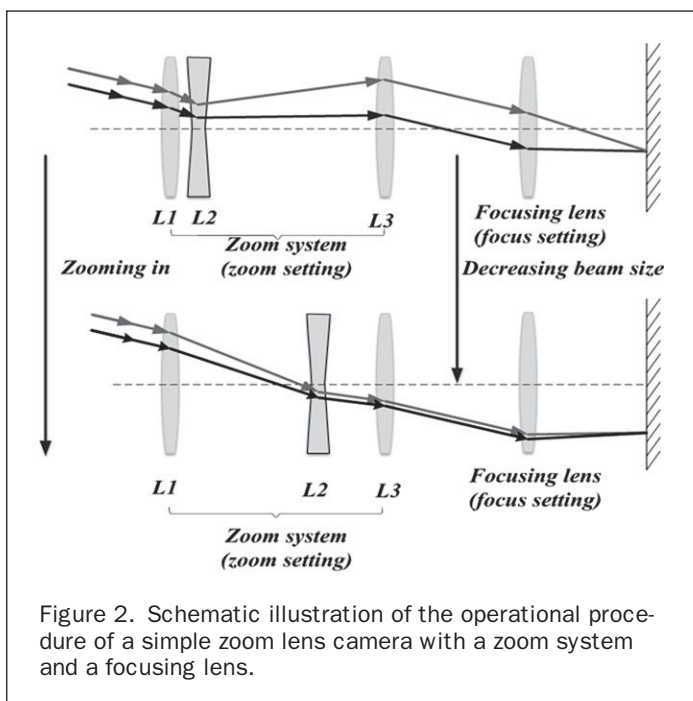

Figure 2. Schematic illustration of the operational procedure of a simple zoom lens camera with a zoom system and a focusing lens.

Overview of the Approach

Camera calibration using only coplanar control points will lead to unstable or non-unique solutions. This is mainly due to the projective couplings between the camera IO and EO parameters, such as the significant correlations between the locations of the principal point and the camera perspective center, and the correlations between the principal distance and the camera depth. As illustrated in Figure 3, when the control points are distributed on a plane M, from the same two images P and P', two or more solutions exist for camera calibration. Figure 3a indicates that with the same image coordinates abc and $a'b'c'$ of the coplanar control points A, B, and C, two pairs of principal point offsets (o and o') and camera perspective centers (S and S') can be estimated. Figure 3b illustrates the non-unique solutions for the principal distance f and the EO parameter Z_S from the coplanar control points.

In order to solve the above problems for camera calibration using a coplanar checkerboard, the following two strategies are developed in this study. First, instead of modeling the variations of principal point offsets with respect to zoom and focus changes, this study fixes the principal point to an image position which has physical significance (Willson, 1994; Li and Lavest, 1996) as an approximation through a focus-of-expansion approach. Second, several sets (at least three) of checkerboard images with different distances from the camera are acquired and used to form a sound geometrical configuration, so that the correlations between the principal distance and the camera depth can be relieved. In addition, to compensate the influences of focus changes on the principal distance and enable the autofocus capability in order to solve the DOF problem at varying distances aforementioned, a scale parameter is employed in the camera model to compensate for influences of focus changes. Based on these strategies, the principal distances are calibrated and distortion parameters are estimated independently for each zoom and focus setting. Finally, polynomials are used to model the principal distance and distortion parameter changes in relation to the various zoom and focus settings. In this approach, the calibration of distortion parameters is separated from calibration of other parameters. This is because of the following reason. To calibrate the principal distance, images with various depths are required to form a robust convergent geometry. To achieve this task, different focus settings have to be applied to capture sharp images due to the limited depth of field. An effective method as mentioned above has been developed to compensate the variations of principal distance caused by different focus settings, however, for distortions there is no such a compensation strategy. Instead, the distortions are calibrated in a separate step while keep others fixed following a strategy similar with the one reported by Brauer-Burchardt and Voss (2001). Figure 4 shows the approach framework.

Three lenses are employed in this study for method development and validation purposes. The first one is a 10 × motorized C-mount zoom lens (Edmund NT57-708) with a CMOS video camera. The focal length of the zoom lens ranges from 12 to 120 mm, and the corresponding field of view (FOV) ranges from 29.4 to 3.1 degrees, respectively. The working distance (the focusable object distance) ranges from 1.5 m to infinite. The lens is zoom and focus controllable with a lens controller. The motorized settings for both the zoom and focus range from 186 to 712 (only 200 to 700 are used in this study for mechanical stability consideration). The camera can record images or video data at resolutions of 1,280 × 1,024 pixels. The pixel size is 5.3 × 5.3 µm. This motorized zoom lens is used to illustrate the detailed calibration method proposed in this paper. To test the practical flexibility of the proposed approach, other two lenses are also studied in the experiments with the same single lens reflex (SLR) camera
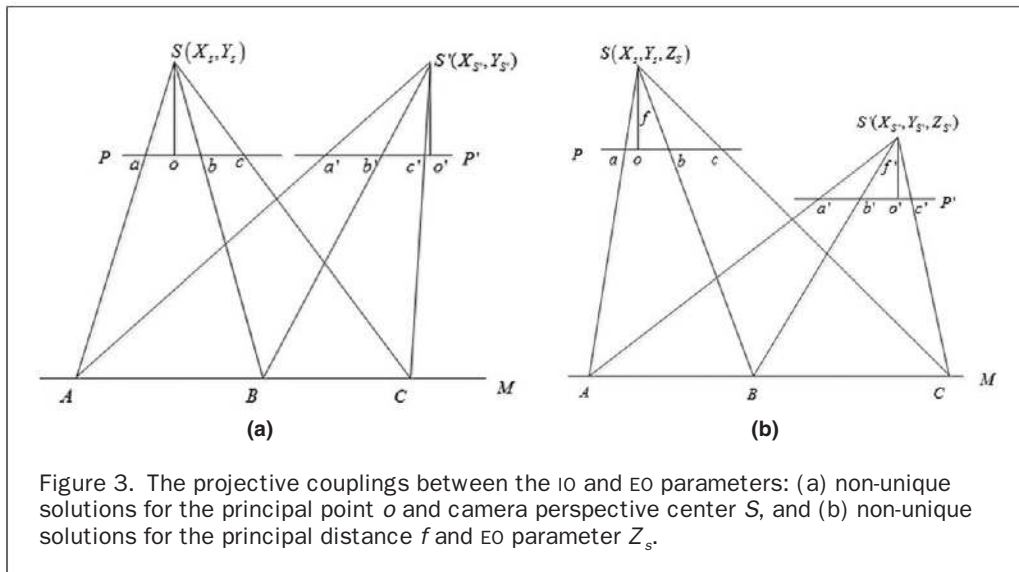
Figure 3. The projective couplings between the IO and EO parameters: (a) non-unique solutions for the principal point o and camera perspective center S, and (b) non-unique solutions for the principal distance f and EO parameter Z_s.
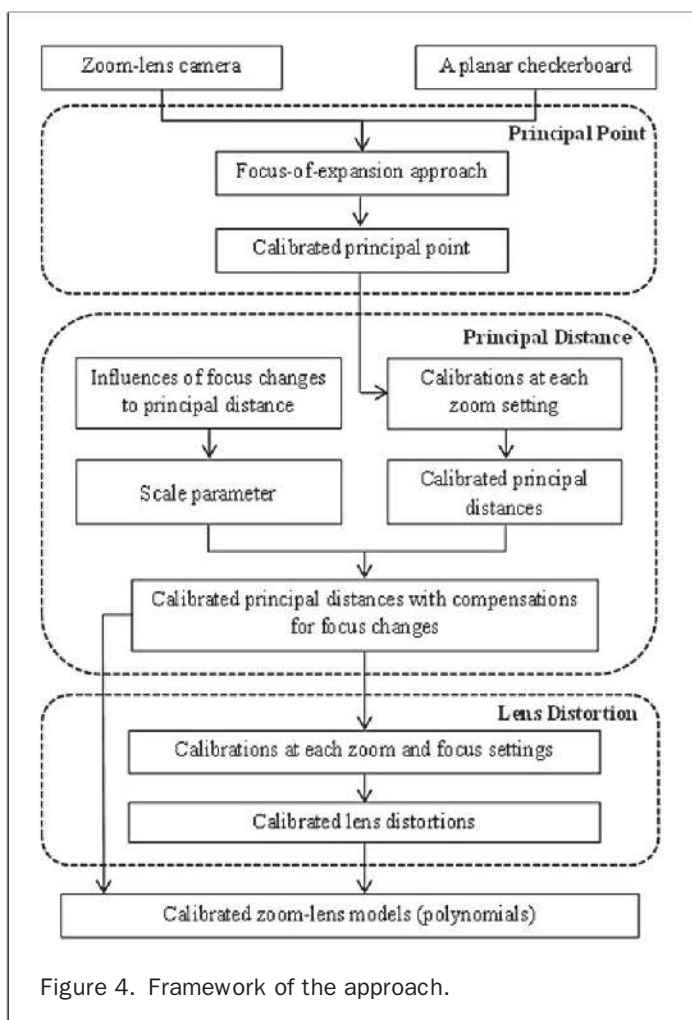

Figure 4. Framework of the approach.

body Canon EOS 5D, which include a Canon EF 28-105 mm f/3.5-4.5 zoom lens and a Canon EF 24 mm f/2.8 prime lens. The pixel size is $8.2\,\mu\text{m} \times 8.2\,\mu\text{m}$. Both of them have the ability of autofocus. The focused distance is recorded from the focus

ring manually. The planar checkerboard used in this study is a 300×420 mm alloy board. A 10×14 grid is engraved precisely on the board. Each cell is 30×30 mm (see Figure 6).

Camera Calibration Model
A camera calibration model for zoom lenses using coplanar control points based on the collinearity equation (Wang, 1990) is developed in this study. The calibration model takes account for the following calibration parameters, the principal point offset (x_0, y_0), principal distance c, radial distortion parameters k_1, k_2, k_3 and decentering distortion parameters p_1, p_2, which are zoom and focus relevant. The relationship between a 3D object point $P(X, Y, Z)$ and the corresponding 2D image point $p(x, y)$ is then modeled by Equation 1:

$$\bar{x} + \Delta x = -cs\frac{a_1(X-X_s)+b_1(Y-Y_s)+c_1(Z-Z_s)}{a_3(X-X_s)+b_3(Y-Y_s)+c_3(Z-Z_s)}$$

$$\bar{y} + \Delta y = -cs\frac{a_2(X-X_s)+b_2(Y-Y_s)+c_2(Z-Z_s)}{a_3(X-X_s)+b_3(Y-Y_s)+c_3(Z-Z_s)}$$

$$\bar{x} = x - x_0, \bar{y} = y - y_0$$

$$r = \sqrt{\bar{x}^2 + \bar{y}^2}$$

$$\Delta x = \bar{x}(k_1 r^2 + k_2 r^4 + k_3 r^6) + [p_1(r^2 + 2\bar{x}^2) + 2p_2\overline{xy}]$$

$$\Delta y = \bar{y}(k_1 r^2 + k_2 r^4 + k_3 r^6) + [p_2(r^2 + 2\bar{y}^2) + 2p_1\overline{xy}]$$

(1)

where (a_i, b_i, c_i) and (X_S, Y_S, Z_S) represent the respective camera orientation and position components. The parameter s is a scale parameter used to compensate for the influences of focus changes on the principle distances (details are discussed in a following section).

After linearization of Equation 1, the observation equations for the bundle adjustment can be derived. To consider the uncertainty propagation of the derived parameters in the sequential steps, this paper employed a strategy by incorporating the IO parameters (principle point and principle distance) as unknowns in the bundle adjustment process but with additional weighted virtual observations. A general expression of the observation equations of the bundle adjustment is listed below:

$$V = At + BX_1 + CX_2 - L, P$$
$$V_{X1} = \qquad X_1 \qquad - L_{X1}, P_{X1}$$

(2)

where t, X_1 and X_2 represent the unknown values for EO, IO and additional distortion parameters, respectively, V is the image points residual, V_{X1} corresponds to the virtual observations for IO, P and P_{X1} are the *a priori* weights to each observation. For the weights of image point observations, a normal matching accuracy of 0.3 pixels is used. For the virtual observations related to the IO, their posteriori uncertainties from preceding bundle adjustment process are used to determine their corresponding weights. Through this way, the uncertainties of all the EO, IO, and distortion parameters can be finally estimated. The initial values for principal distance are interpolated from the nominal minimum and maximum focal lengths of the zoom lenses. For the distortion parameters, their initial values are set to zero.

At each individual zoom and focus settings, the calibration parameters can be solved through a bundle adjustment process using Equations 1 and 2. The bundle adjustment is based on a least squares approach. The above method is adopted to obtain the calibration parameters at a series of discrete zoom and focus settings covering the entire lens control ranges. The variations of the calibration parameters are then modeled empirically, by polynomials.

Principal Point

The principal point is defined as the "point on the image plane at the base of the perpendicular from the center of the lens, or more correctly, from the rear nodal point" (Fryer, 1996). Instead of modeling the principal point offsets as a function of the zoom and focus settings such as those reported in previous work (Willson, 1994; Wiley and Wong, 1995; Fraser and Al-Ajlouni, 2006), this study fixes the principal point to an image point relevant to the zoom and focus settings. The reasons are as follows: (a) The variations of the principal point offset are not significant, and no common variation trend could be derived for different cameras. Practical ways to calibrate the principal point are to use a best-fit linear variation function or to simply fix the principal point relevant to the zoom and focus settings (Li and Lavest, 1996); (b) The couplings between the principal point offset and other parameters may cause defects in the bundle adjustment process and thus lead to unstable calibration results, especially at large focal lengths (Clarke *et al.*, 1998); (c) The effects of projective compensations between image IO and EO parameters indicate the need to simply fix the principal point to a physically significant image point. Previous experimental results have proved that a deliberate shift of the principal point can be compensated for by EO parameters (Tsai, 1987; Fryer, 1998).

To determine the principal point of the zoom lens, a focus-of-expansion technique is employed in this study. First, a series of images are taken over a range of zoom settings with the object plane and camera held fixed. The trajectories of the same target point are then tracked and fitted to a line (Figure 5). All the trajectories of the target points intersect at an image center, which is the focus-of-expansion. Figure 5 illustrates the focus-of-expansion process.

Figure 6 shows the results of the focus-of-expansion process using the Edmund NT57-708 motorized zoom-lens camera and the planar checkerboard. The camera and the checkerboard are both held fixed. A series of checkerboard images are taken across the whole zoom setting span as shown in Figure 6a. The trajectories of each grid point in the checkerboard are tracked and intersect at the focus-of-expansion as illustrated in Figure 6b.

To examine the stability of the focus-of-expansion determined using the above approach, different focus settings ranging from 200 (focus at infinite) to 700 (focus at about 1.5 m) are employed in the above experiments, and their corresponding focuses-of-expansion are determined, respectively, as

shown in Table 1. It should be noted that, some zoom settings are deliberately ignored in the experiments, e.g., large zoom settings when using close focus and small zoom settings for far distance if tracking targets are too vague to be detected or too few targets can be tracked.

As can be seen from Table 1, the determined focuses-of-expansion with different focus settings and different object distances are quite stable (with a standard deviation of 0.002 mm). Therefore, this study takes the average value of
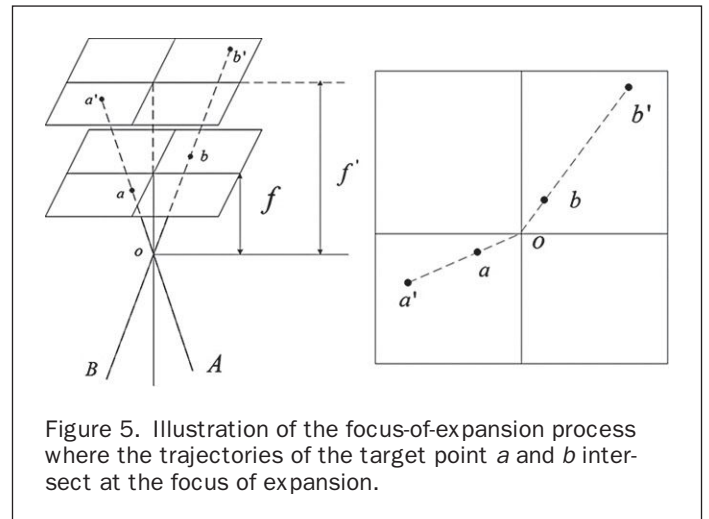

Figure 5. Illustration of the focus-of-expansion process where the trajectories of the target point *a* and *b* intersect at the focus of expansion.
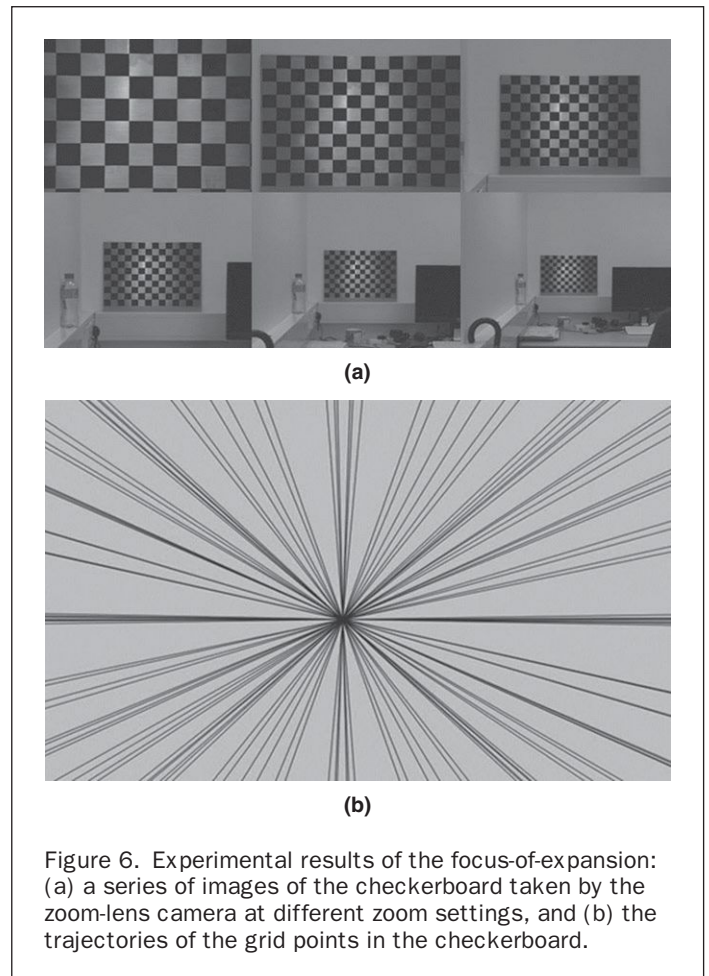

(a)

(b)

Figure 6. Experimental results of the focus-of-expansion: (a) a series of images of the checkerboard taken by the zoom-lens camera at different zoom settings, and (b) the trajectories of the grid points in the checkerboard.

TABLE 1. FOCUSES-OF-EXPANSION AT DIFFERENT FOCUS SETTINGS

Focus settings	Involved zoom settings	Involved grid points	Determined focuses of expansion (x0, y0) (mm)
200	400, 500, 600, 700	13×9	3.4720, 2.8369
300	300, 400, 500, 600, 700	12×8	3.4736, 2.8356
400	200, 300, 400, 500, 600, 700	9×7	3.4754, 2.8410
500	200, 300, 400, 500, 600	13×9	3.4726, 2.8380
600	200, 300, 400, 500, 600	13×9	3.4748, 2.8372
700	200, 300, 400, 500, 600	9×7	3.4734, 2.8383

the focuses-of-expansion across different focus settings as the principal point.

To validate the effectiveness of determining the principle point through the focuses-of-expansion strategy, this paper investigates the principal point wander through experimental analysis using the Canon EF 28-105 mm zoom lens. Self-calibration processes were performed for the zoom lens in an indoor control field to obtain the accurate principle points at different zoom and focus settings covering their entire settings. The precision of the calibrated principal points is about one pixel. Figure 7 shows a contour plot of the obtained principle points (x_0, y_0) with respect to various zoom and focus settings. As expected, Figure 7 shows the random distribution of calibrated principle points, which is consistent with the investigation by Fraser and Al-Ajlouni (2006). In addition, this experimental analysis confirmed that the randomness not only exists in variation of zoom but also of focus. The maximum range of the principal point variations determined through the self-calibration approach across the entire zoom and focus settings is 0.3 mm (36.6 pixels). The discrepancy between the principal point determined by the focus-of-expansion approach and the self-calibration approach is 10.2 pixels in average for the tested zoom and focus settings.

To quantitatively characterize the significance of the principal point wander, five different types of principal point determination were tested and examined at a specific zoom setting of 75 mm and focus setting of 0.25 (4 m). The first one is the principal point determined through the self-calibration approach as mentioned above. The second one is determined by the focuses-of-expansion strategy proposed in this paper. The third one is obtained from a first-order polynomial derived from the calibrated principle points across various zoom and focus settings as shown in Figure 7. The forth one deliberately adds a 10 pixels shift to the self-calibration results. The fifth one directly locates the principal point at the image center, which is about 40 pixels shift to the self-calibration results. The principal point is fixed during the bundle adjustment process. In order to focus solely on the impact of principal point, all the other intrinsic parameters are estimated in a self-calibration means. Dozens of independent check points in the control field are used to evaluate the performances of the five types of principal points. RMSE (root mean-square error) against the true 3D coordinates of the check points and RMSE of the residuals in image space are recorded and summarized in Table 2.

From Table 2, it can be seen that the small errors in principal point can be compensated by EO parameters after the bundle block adjustment, which agrees with the reports from Tsai (1987) and Fryer (1998). Several pixels inconsistencies in the principle points determined by the focuses-of-expansion approach and the forst-order polynomial only result in about 0.002 mm accuracy loss compared with the results from the self-calibration method. More quantitative evaluations can be seen in the results from Type 4 when deliberately shifting the principal point determined by the self-calibration method to 10 pixels away, and Type 5 when directly fixing it at the image center (about 40 pixels shift to the self-calibration results). Although the outcomes degenerate a little, they still remain reasonable. The above analysis proved that the proposed focus-of-expansion approach is valid and effective.

Principal Distance
Formation of Convergent Image Geometry Using the Checkerboard
Principal distance is defined as the perpendicular length from the perspective center of the camera to the principal point
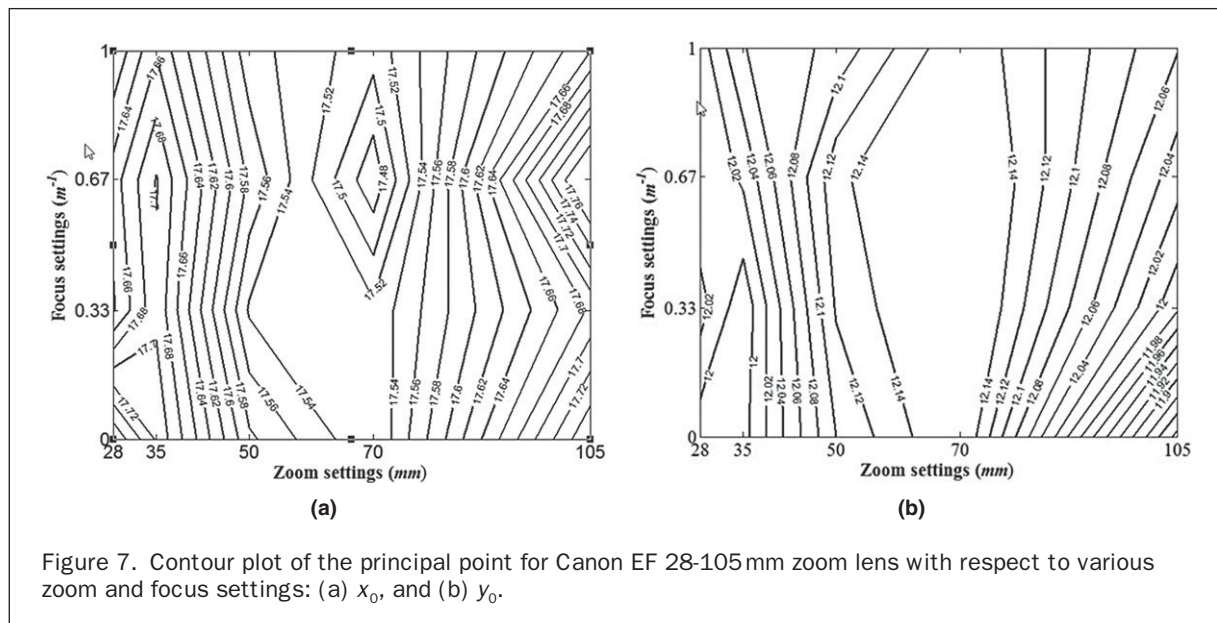

Figure 7. Contour plot of the principal point for Canon EF 28-105 mm zoom lens with respect to various zoom and focus settings: (a) x_0, and (b) y_0.

Types	Principal Point(mm)		RMSE of 3D Coordinates (mm)	RMSE of Image Residuals (pixels)
	x_0	y_0		
1. Self-calibration	17.5596	12.0363	0.1575	0.1330
2. Focuses-of-expansion	17.6128	11.9575	0.1589	0.1348
3. First-order polynomial	17.6501	12.0398	0.1602	0.1346
4. 10 pixels shift to type 1	17.6416	12.1183	0.1631	0.1361
5. Image center (about 40 pixels shift to type 1)	17.9088	11.9392	0.1720	0.1549

(Fryer, 1996). In order to determine the principal distance in the camera calibration process, convergent image geometric configurations are necessary bearing in mind the strong correlations between the principal distance and the depth of the camera (i.e., the Z_s of the EO parameters) as mentioned above. This is especially so, when the calibration targets are coplanar such as the study case presented in this paper. Zhang (2000) proved that in theory three checkerboard images are enough for accomplishing the calibration. However in the practice in this study, we found that more images are necessary for obtaining accurate and stable results which agrees with the statements in Sturm *et al.* (2011).

An experimental analysis was carried out to investigate the formation of convergent image geometry from the checkerboard images. Five sets of checkerboard images with various distances from the camera were taken (Set 1: a distance of 7.5 m to the camera, Set 2: 6.0 m, Set 3: 4.5 m, Set 4: 3.3 m, and Set 5: 2.5 m). Each set includes four images with different rotation and roll angles. Calibration process was performed for each set of images first, and the principal distances were determined for the five sets of images. Random image set combinations (combining two to five sets) were then employed and the corresponding principal distances were also obtained. Table 3 shows the total 15 principal distances derived using different image sets.

From Table 3, it can be seen that the derived principal distances using one or two individual image set are not stable. Stable results, however can be expected after using three sets of images. This can be explained by the fact that the use of three or more planar checkerboard image sets can create proper convergent image geometry and relieve correlation problems between the principal distance and Z_s, hence obtaining more stable results. Based on experimental analyses

TABLE 3. PRINCIPAL DISTANCES DERIVED FROM DIFFERENT COMBINATIONS OF IMAGE SETS

Image sets (one set)	1	2	3	4	5
Principal distance c (mm)	37.782	36.584	36.661	36.120	37.492
Image sets (two sets)	1 & 4		1 & 5		2 & 3
Principal distance c (mm)	36.175		37.495		36.653
Image sets (three sets)	1, 3, & 5		2, 4, & 5		3, 4, & 5
Principal distance c (mm)	37.066		37.068		37.067
Image sets (four sets)	1, 2, 4, & 5		1, 3, 4, & 5		2, 3, 4, & 5
Principal distance c (mm)	37.073		37.072		37.058
Image sets (five sets)	1, 2, 3, 4, & 5				
Principal distance c (mm)	37.063				

in this study, at least three sets of checkerboard images (about 2 m distance interval when taking the three sets of images) with different rotation or roll angles in each set is recommended for zoom-lens calibration use.

Influences of Focus Changes to Principal Distance
As mentioned above, stable principal distance can be obtained by using coplanar targets with varying distances to the camera and large convergent angles, however, this has raised another issue that capture of sharp images of calibration targets at various depths with fixed zoom and focus settings is difficult and sometimes impossible, especially in the case of large zoom settings and small focused distances as indicated in Figure 1. For example, for the Edmund NT57-708 motorized zoom lens used in this study, the DOF will not surpass 10 cm with the nearest focus and largest zoom setting under the normal illumination intensity and relatively small iris setting. Therefore, change of focus setting for sharp images at different depths is necessary.

In order to recover principal distances at any zoom and focus settings, an effective strategy to normalize the principal distance to a reference focus setting (the one which represents infinity focus), is developed in this study. For each zoom setting, a scale parameter is used to model the relative variations of the principal distances in relation to the principal distance at the pre-defined reference focus setting caused by the focus variations. The scale parameter has a similar physical meaning with the image scale c/Z_S if Z_S (the distance from the camera to the target) held fixed. Based on similar triangles, the variations of the principal distance c caused by the variations of focus can be considered as the variations of the length of the image plane, if the EO parameter Z_S is held fixed.

Experimental analysis is carried out to examine the scale parameter. With the positions of the checkerboard and the camera both fixed, a series of checkerboard images are taken at each zoom setting with different focus settings across the whole zoom and focus control ranges. Figure 8 gives an example of the image series captured by the motorized zoom lens with a zoom setting of 600 (a focal length about 55 mm) and various focus settings from 200 to 700.

For the convenience of implementation, the diagonal lengths of the checkerboard in the images are measured at each zoom and focus settings. The lengths are then normalized to the reference focus setting of 200 for each zoom setting with scale parameters. The detailed results are shown in Table 4, from which the following two general tendencies can be concluded. First, the scale parameter monotonically increases as the focus setting increases at each fixed zoom setting. Second, the influences on principal distance from focus changes are more apparent on larger zoom settings, e.g., 20 percent on zoom setting 600.
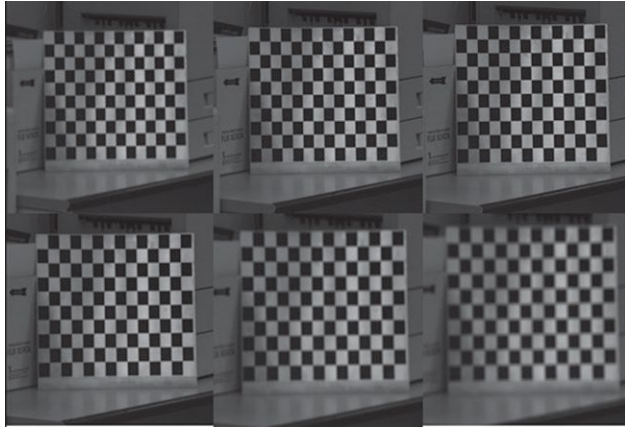
Figure 8. Images of the checkerboard with a zoom setting of 600 and various focus settings from 200 to 700 (from top-left to bottom-right).

A bivariate n^{th} order polynomial is employed to model the scale parameter $s(z, f)$ for the zoom lens by Equation 3:

$$s(z,f) = \sum_{i=0}^{n} \sum_{j=0}^{i} a_{ij} z^{i-j} f^{j} \qquad (3)$$

where z and f represent the zoom and focus settings, respectively. The order of the polynomial is dependent on both the practical experience and number of calibrated lens settings.

In the above description, a reference focus setting of 200 is used as the scale factor base for the Edmund NT57-708 motorized zoom lens. The focus setting of 200 for this zoom lens is corresponding to an infinite focused distance. For other zoom-lens cameras, a similar scale factor base corresponding to an infinite focused distance can be decided.

It should be noted that, the tiny influences on object distance (Z_S) caused by the changes of focus settings are ignored in determining the scale parameter. This is because the object distance is generally in the magnitude of several meters, while the changes of Z_S caused by the focus settings are in magnitude of millimeters. Additionally, this type of tiny offsets can hardly be measured accurately. Omission of this type of tiny offsets is acceptable as supported by the experimental results given in the *Experimental Results and Analysis* Section that follows.

Principal Distance Modeling for Zoom Lens
Once the scale parameter is determined with a specific zoom and focus settings, a zoom-dependent calibration process of

the normalized principal distance can be carried out using auto-focus images from varying distances. A polynomial $c(z)$ is used to model the variations of the principal distance as:

$$c(z) = \sum_{i}^{n} a_i z^i. \qquad (4)$$

It should be noted that, the correction of lens distortions has been ignored in this step. Experimental results show that with or without lens distortion correction there is no notable differences in the derived principal distances. The characteristics of the principal distance modeling in this study have much in common with previous investigations on zoom lens systems (Willson, 1994; Li and Lavest, 1996).

Finally, the principal distance $c'(z, f)$ of the zoom lens under any zoom and focus settings is determined by Equation 5.

$$c'(z, f) = c(z)\, s(z, f). \qquad (5)$$

Lens Distortion
With the principal point and principal distance determined through the process discussed above, the coupling problem between the IO and EO parameters is eliminated, and in theory, only one image of the checkerboard is needed to derive the distortion parameters. In practice, several images cover the whole image scope are used to calibrate the lens distortions.

Although there will be different radial distortions for images with different focused object distance (Brown, 1971), and even in the same image, different object distances will result in various radial distortions; however, variation in radial distortion of different object distance is only significant at large image scales. Since the goal of this study is to calibrate the zoom lens through a flexible approach, this study tries to empirically model the distortion parameters by polynomials.

For the Edmund NT57-708 motorized zoom lens and camera system, the sensing area is relatively small ($6.79\,mm \times 5.43\,mm$) compared with the SLR cameras (e.g., the sensing area is $35.8\,mm \times 23.9\,mm$ for the Canon EOS 5D), and a narrow field of view is companied with small sensor. Experimental results in this study indicate that both radial and decentering distortions are, to some extent, smaller for the Edmund NT57-708 motorized zoom lens and camera system. Therefore, for this lens the radial distortion parameters, as given in Equation 1, only k_1 is adopted for practical and convenient considerations, as suggested by Fryer (1996). For the decentering distortions, although some of the previous studies suggest the employment of the decentering distortion parameters in distortion calibration for zoom lenses (Wiley and Wong, 1995), many other studies (Li and Lavest, 1996; Fraser and Al-Ajlouni, 2006) have proved that the omission of the decentering distortion parameter p_1 and p_2 has little impact on the metric accuracy. This is mainly because decentering

TABLE 4. DIAGONAL LENGTHS OF THE CHECKERBOARD AND NORMALIZED SCALES

	Zoom 200		Zoom 300		Zoom 400		Zoom 500		Zoom 600	
	Length	Scale	Length	Scale	Length	Scale	Length	Scale	Length	Scale
Focus 200	337.4	1.00	428.7	1.00	575.1	1.00	807.4	1.00	890.9	1.00
Focus 300	342.5	1.02	435.8	1.02	587.0	1.02	827.0	1.02	920.5	1.03
Focus 400	347.6	1.03	443.7	1.04	599.0	1.04	848.8	1.05	952.1	1.07
Focus 500	352.9	1.05	451.5	1.05	611.8	1.06	870.4	1.08	986.3	1.11
Focus 600	358.6	1.06	460.0	1.07	625.8	1.09	895.5	1.11	1023.2	1.15
Focus 700	364.4	1.08	468.6	1.09	640.1	1.11	921.4	1.14	1065.0	1.20

distortion is generally small, for instance, no more than 0.5 pixels of decentering distortion have been found for the Edmund NT57-708 motorized zoom lens used in this study. Therefore, decentering distortions have been ignored for the Edmund NT57-708 lens in this study. While for the other two lenses, the Canon EF 28-105 zoom lens and Canon EF 24 mm prime lens, they have a relatively larger sensing area, and the radial distortion may have a higher order changing behavior, and the decentering distortion may increase to several pixels. Therefore, four additional parameters k_1, k_2, p_1, and p_2 are utilized for modeling image distortions for these two lenses.

Several sets of checkerboard images with various zoom and focus settings covering the entire lens control range were taken and used for lens distortion calibration. To model the distortion parameter k and p for the zoom lens, the following polynomials are used:

$$k = \sum_{i=0}^{n} \sum_{j=0}^{i} a_{ij} z^{i-j} f^j, \quad p = \sum_{i=0}^{n} \sum_{j=0}^{i} a_{ij} z^{i-j} f^j. \quad (6)$$

Experimental Results and Analysis

Three different types of lens, Edmund NT57-708 motorized zoom lens, Canon EF 28-105 zoom lens, and Canon EF 24 mm prime lens, were calibrated using a planar checkerboard with explicit methods. The internal parameters, including principal distance and distortion parameters were modeled by polynomials. The calibration results are presented and analyzed in following in detail. Accuracy evaluation is further conducted against the self-calibration method and the well-known Zoom-dependent technique.

Calibration and Modeling Results

The calibrations were conducted among the whole span of the zoom/focus settings. For the Edmund NT57-708 motorized zoom lens, zoom and focus readings were recorded with vendor-provided APIs. For the two Canon lenses, zoom settings were recorded in the EXIF header and focused distances were estimated from the lens manually, and reciprocal of the focused distance was deemed as focus setting (e.g., focus setting 0 represents infinite focused distance).

Results of Principal Point

For the two zoom lenses, the Edmund NT57-708 motorized zoom lens and the Canon EF 28-105 zoom lens, focus-of-expansion has been derived at each focus setting using the approach previously presented. The results are shown in Figure 9; no evident trait can be concluded from Figure 9. The random change is not to a significant extent. The erratic variation with zoom or focus setting has also reported by others (Wiley and Wong, 1995; Fraser and Al-Ajlouni, 2006). Therefore, the average is taken and fixed as principal point relying on the error compensation by EO parameters in bundle adjustment. For the Canon EF 24 mm prime lens without zoom ability, simply using the image center or self-calibration value at one specific focus setting is sufficient on the assumption that random and small variation is caused by focus.

Results of Principal Distance

Figure 10 illustrates the variations of the scale parameters across the entire zoom and focus settings for the three lenses studied, from which it can be seen that the scale parameter should be modeled using different functions for different
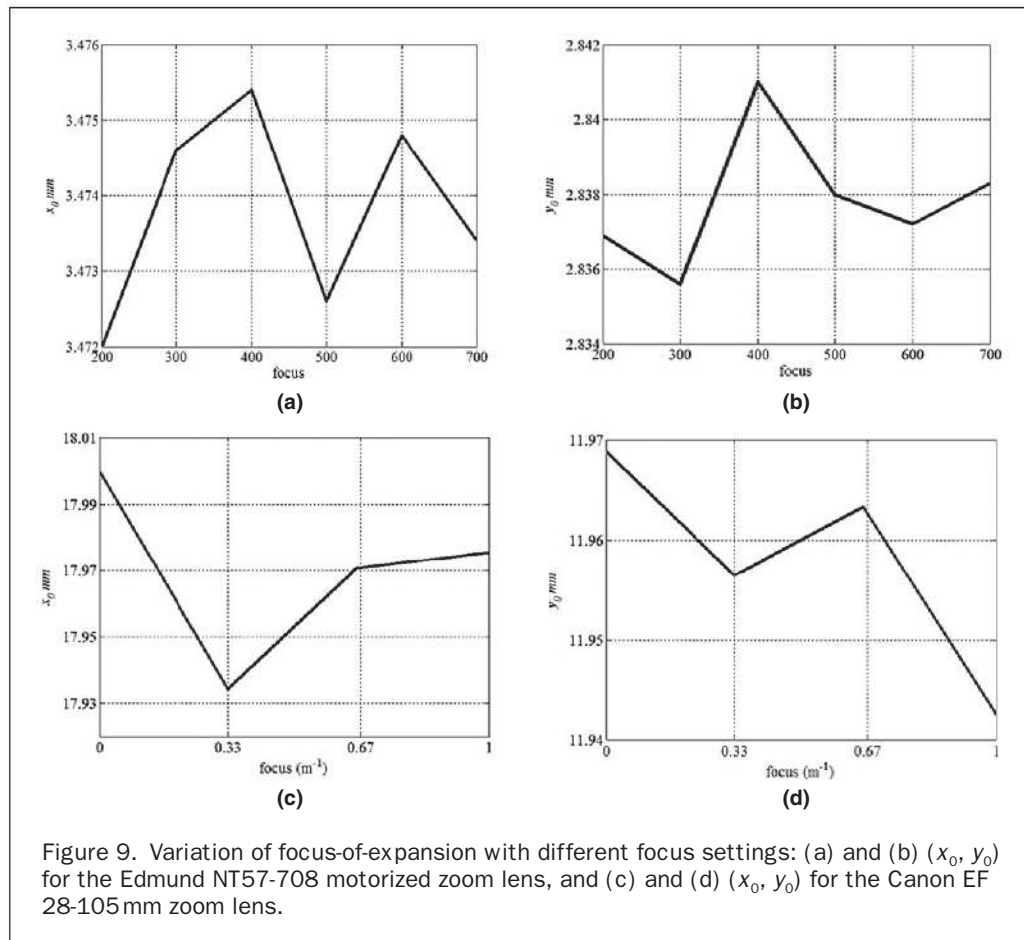

Figure 9. Variation of focus-of-expansion with different focus settings: (a) and (b) (x_0, y_0) for the Edmund NT57-708 motorized zoom lens, and (c) and (d) (x_0, y_0) for the Canon EF 28-105 mm zoom lens.
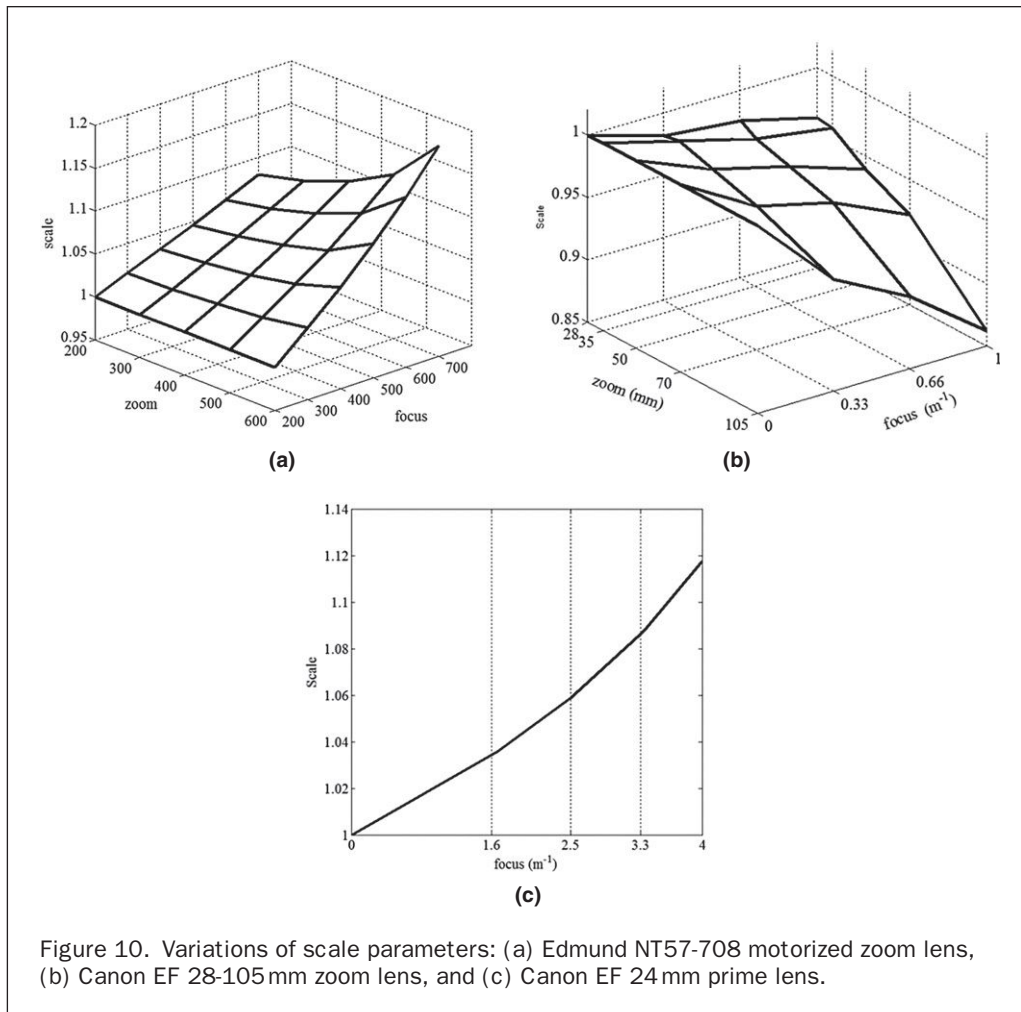
Figure 10. Variations of scale parameters: (a) Edmund NT57-708 motorized zoom lens, (b) Canon EF 28-105 mm zoom lens, and (c) Canon EF 24 mm prime lens.

lenses. For the Edmund NT57-708 motorized zoom lens, a bivariate second-order paraboloid is used to fit the scale variations, however for the Canon EF 28-105 mm zoom lens and Canon EF 24 mm prime lens, the first-order polynomials (plane and line) are used, respectively. From Figure 10, it can be seen that not only the order of polynomials is different, but also the variation tendency. The scale decreases with increasing focus setting for the Canon EF 28-105 mm zoom lens which is alien to the other two lenses. On comparing the Edmund NT57-708 motorized zoom lens and the Canon EF 28-105 mm zoom lens, one common feature is noticed: the influences on principal distances from focus changes are more apparent at larger zoom settings. Similar characteristics of the influences of focus changes on principal distance for motorized zoom lens have also been mentioned by Willson (1994), but to our knowledge, no similar investigation for an off-the-shelf camera has been studied before.

Shown in Figure 11 are the normalized principal distances for the Edmund NT57-708 motorized zoom lens and the Canon EF 28-105 mm zoom lens. For the Canon EF 24 mm prime lens, the calibrated principal distance is 24.414 mm at infinity focus. The uncertainties of the calibrated normalized principal distance at all zoom/focus settings are superior to 0.1 percent. Again, different lens behavior can be seen, and polynomials with various orders are used, e.g., for the Edmund NT57-708 motorized zoom lens, a quartic polynomial is used because three inflection points are noticed on the curve shown in Figure 11a. On the other hand, a line is used

for the Canon EF 28-105 mm zoom lens because the normalized principal distance is quite close to the effective focal length obtained in the EXIF header. The principal distance is then modeled by Equation 5 at any zoom and focus settings.

Results of Lens Distortions
Figures 12, 13, and 14 describe the variations of lens distortion parameters for the three lenses studied in this paper. The monotonic decrease with increasing zoom for the cubic component of radial distortion k_1 shown in Figures 12, Figure 13a, and Figure 14a has also been reported by others (Wiley and Wong, 1995; Laebe and Foerstner, 2004; Fraser and Al-Ajlouni, 2006). The distortion parameters are modeled using bivariate quadratic polynomials for the Edmund NT57-708 motorized zoom lens and the Canon EF 28-105 mm zoom lens. For the Canon EF 24 mm prime lens, focus-dependent models are studied, and linear and parabolic models are used for the radial and decentering distortion parameters, respectively. As noticed from Figures 13 and 14, variations of p_1, p_2 are less regular than that of k_1 and k_2. This is mainly due to the fact that the decentering distortion is too small so that any perpetuation in the calibration procedure will affect its value to a relatively noticeable extent. The average uncertainties of the calibrated distortion parameters across all the zoom and focus settings are generally less than 2 percent except for that of k_2 (5.06 percent for k_2). Considering the fact that the impact of fifth-order part of radial distortion is rather small, these results can be considered satisfactory.
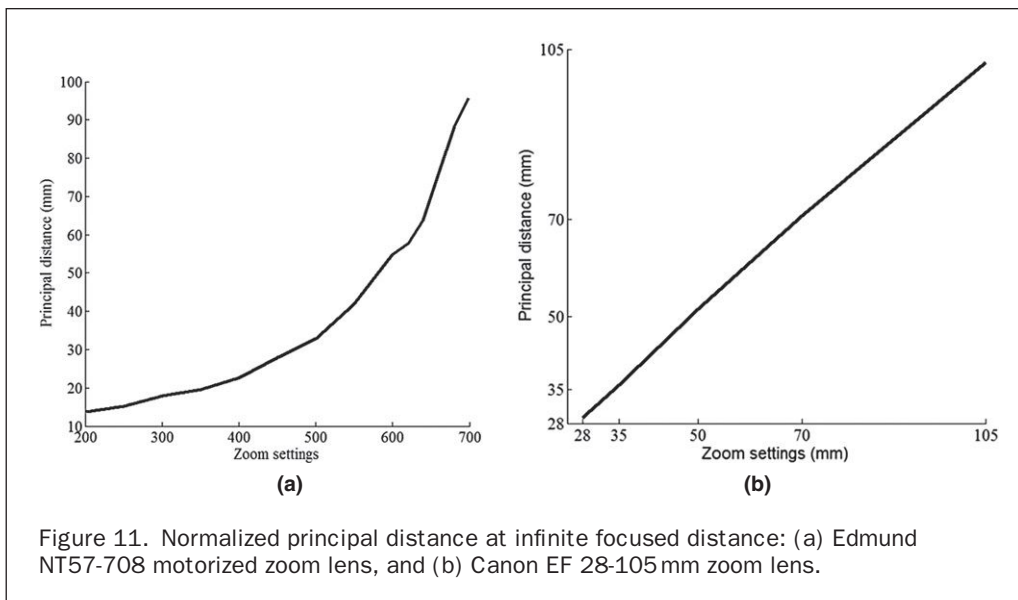
Figure 11. Normalized principal distance at infinite focused distance: (a) Edmund NT57-708 motorized zoom lens, and (b) Canon EF 28-105 mm zoom lens.
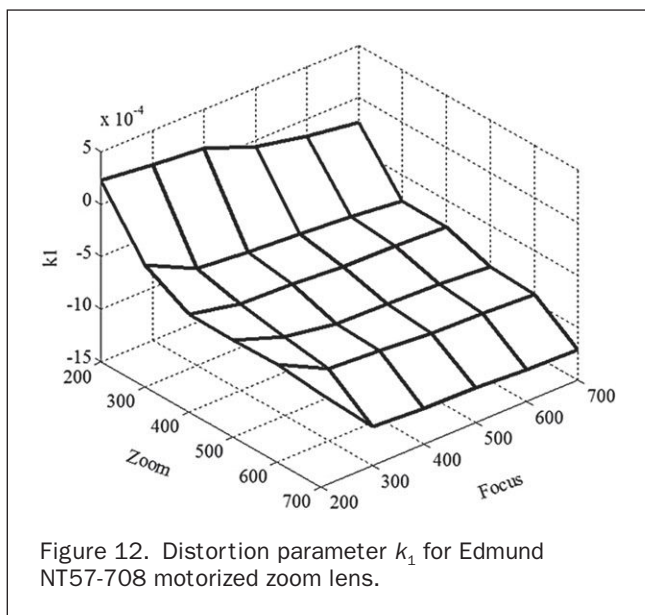

Figure 12. Distortion parameter k_1 for Edmund NT57-708 motorized zoom lens.
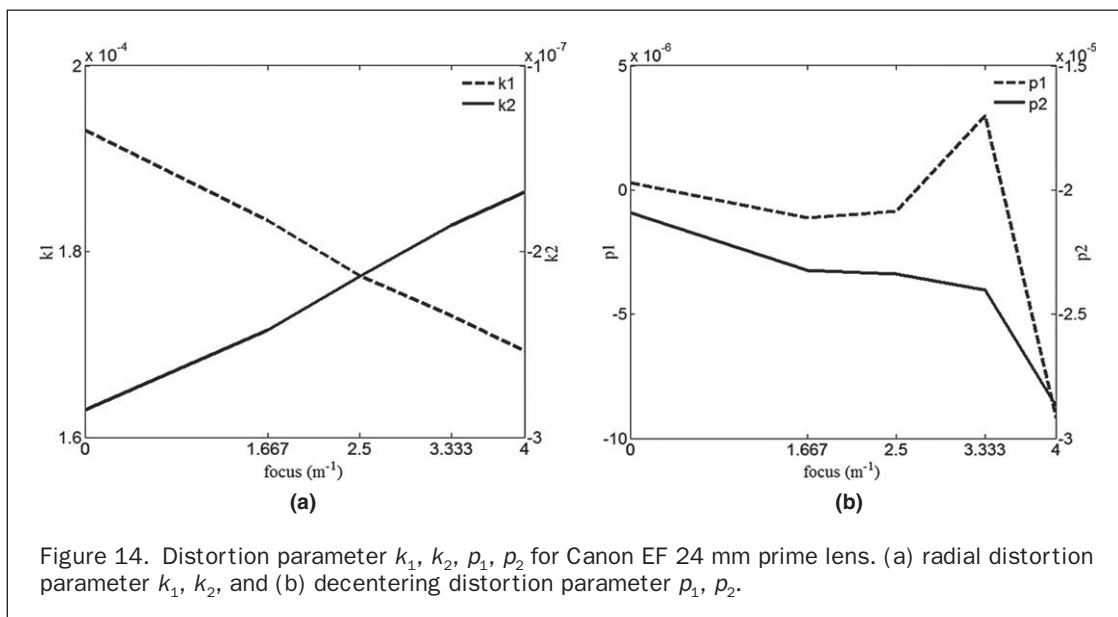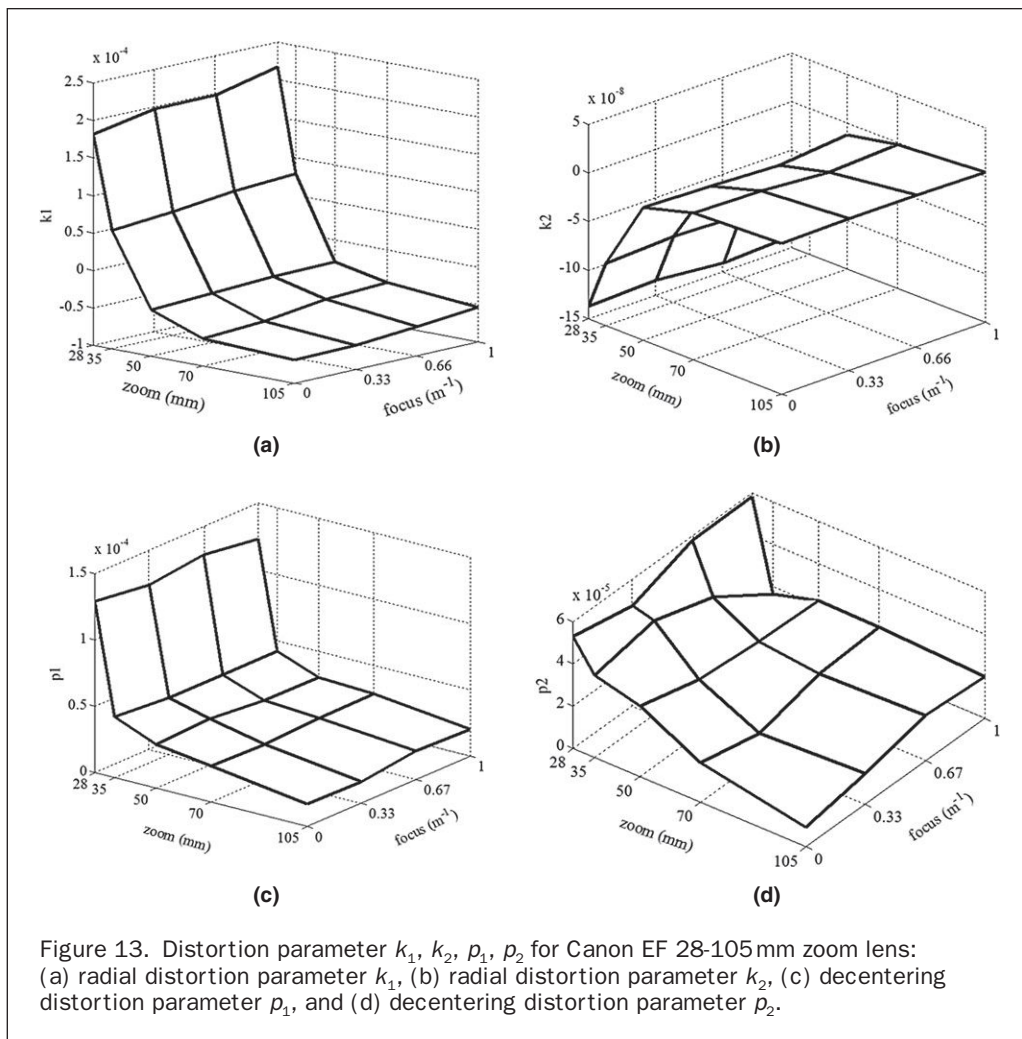
In order to study the zoom and focus effects to distortions, variations of radial distortion with respect to zoom and focus settings are plotted in Figures 15 and 16, respectively. Figure 15 shows the radial distortions on image plane for the Edmund NT57-708 motorized zoom lens and Canon EF 28-105 mm zoom lens under different zoom settings, of which the monotonic decrease and zero-cross are consistent with the works reported by others (Laebe and Foerstner, 2004; Fraser and Al-Ajlouni, 2006). Although zoom is the dominant factor in affecting distortions, the effect from focus cannot be ignored as shown in Figure 16. Figure 16 illustrates the radial distortions at the largest radius on image plane for the three lenses under different focus settings. At some zoom settings, its effect will surpass about 20 percent. Therefore, in these cases modeling of distortions must take focus into consideration.

To investigate the fitness of the mathematical models and the calibrated results, χ^2 tests were performed for the variances of the discrepancies between the mathematical models, and the calibrated results with a given variance at 5 percent significance level. Shown in Table 5 are the χ^2 test results for the Edmund NT57-708 motorized zoom lens and the Canon EF 28-105 mm zoom lens. *H* is the binary indicator indicating which hypothesis is accepted. *P-value* is the probability of observing the given result. Small values of *p* cast doubt on the validity of the null hypothesis. The confidence interval is the range for the true variance under 95 percent confidence.

As indicated in Table 5, all the models except for that of p_1 and p_2 of the Canon EF 28-105 mm zoom lens passed the tests, which means the models and the related data fit each other well. The exceptions of p_1 and p_2 are easy to understand giving the fact that the variation trend of the decentering distortion parameters is rather irregular as shown in Figures 13 and 14. The exceptions of p_1 and p_2 will not affect the overall outcome giving the fact that the decentering distortion is rather small and some previous works even ignored it.

Accuracy Evaluation

A test field is set up for accuracy evaluation of the developed zoom lens models. The object points array, comprised of 864 retro-reflective targets on a wall of 5 m diameter, is measured by using a total station. The 3D positioning precision (mean square error of unit weight) is 0.047 mm. This test field is used for the Canon lenses with circular flashlight. As no flashlight is installed on the Edmund NT57-708 motorized zoom lens, another black-white object points array on a frame of about 1.5 m diameter with 120 coded targets is also employed for tests. The 3D positioning precision for the targets on this frame is 0.029 mm. Figure 17a and 17b show the two object points arrays. Figure 17 also illustrates the representative basic convergent geometry at each zoom and focus setting for self-calibration. Both the measurement of the object points array and accuracy tests are conducted in a 3D close-range photogrammetry software, PhotoModeler®. The intrinsic parameters are determined by Equation 6 using the calibration results for each zoom/focus setting. For each lens, several zoom/focus combinations are chosen

Figure 13. Distortion parameter k_1, k_2, p_1, p_2 for Canon EF 28-105 mm zoom lens: (a) radial distortion parameter k_1, (b) radial distortion parameter k_2, (c) decentering distortion parameter p_1, and (d) decentering distortion parameter p_2.

Figure 14. Distortion parameter k_1, k_2, p_1, p_2 for Canon EF 24 mm prime lens. (a) radial distortion parameter k_1, k_2, and (b) decentering distortion parameter p_1, p_2.
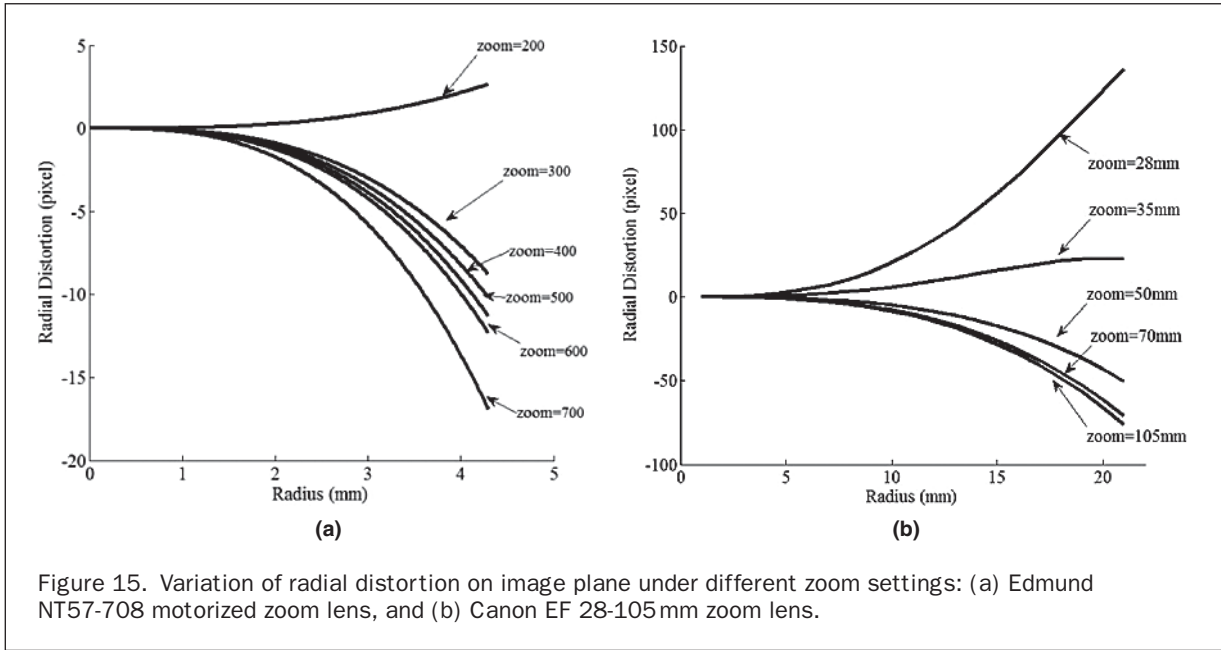
Figure 15. Variation of radial distortion on image plane under different zoom settings: (a) Edmund NT57-708 motorized zoom lens, and (b) Canon EF 28-105 mm zoom lens.
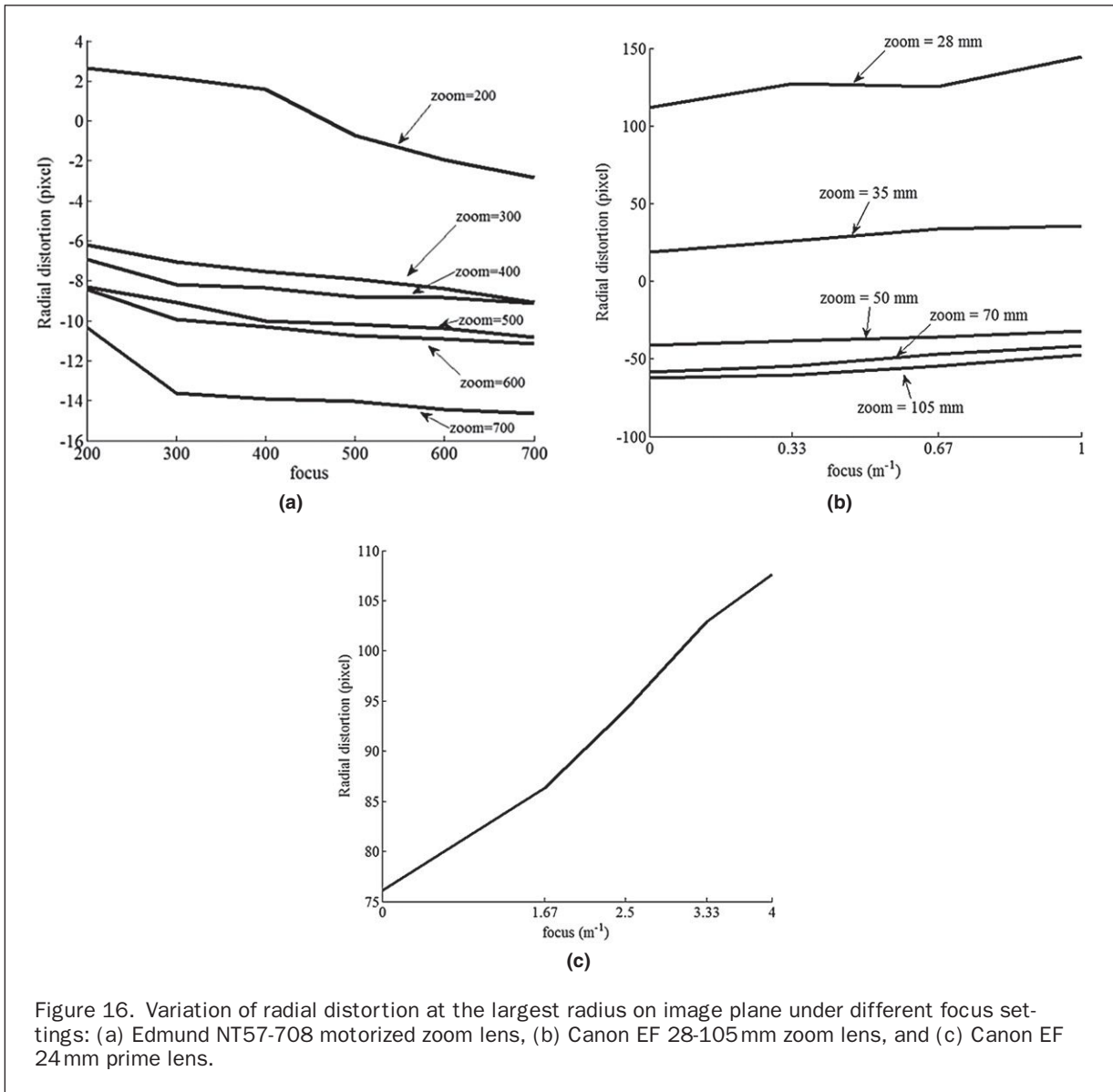

Figure 16. Variation of radial distortion at the largest radius on image plane under different focus settings: (a) Edmund NT57-708 motorized zoom lens, (b) Canon EF 28-105 mm zoom lens, and (c) Canon EF 24 mm prime lens.

TABLE 5. χ^2 TEST RESULTS

| Lens	Model	Discrepancy mean	σ^2	σ_0^2	H	P-value	Confidence interval
Edmund NT57–708 zoom lens	c	−8.55E−11	1.9658	2.6902	0	0.7343	>1.1428
	$scale$	2.97E−14	1.80E−05	1.53E−05	0	0.2336	>1.225e−5
	k_1	6.53E−16	2.59E−09	2.27E−09	0	0.2592	>1.823e−9
Canon EF 28–105 zoom lens	c	1.09E−13	0.0511	2.1381	0	0.9989	>0.0215
	$scale$	−1.61E−15	1.60E−05	2.11E−05	0	0.7614	>1.005e−5
	k_1	6.52E−19	8.60E−10	8.21E−10	0	0.3997	>5.423e−10
	k_2	−2.26E−22	1.53E−16	2.16E−16	0	0.8149	>9.614e−17
	p_1	7.42E−20	4.65E−10	1.27E−10	1	1.16E−07	>2.929e−10
	p_2	−6.83E−20	4.92E−11	6.01E−12	1	1.67E−23	>3.103e−11
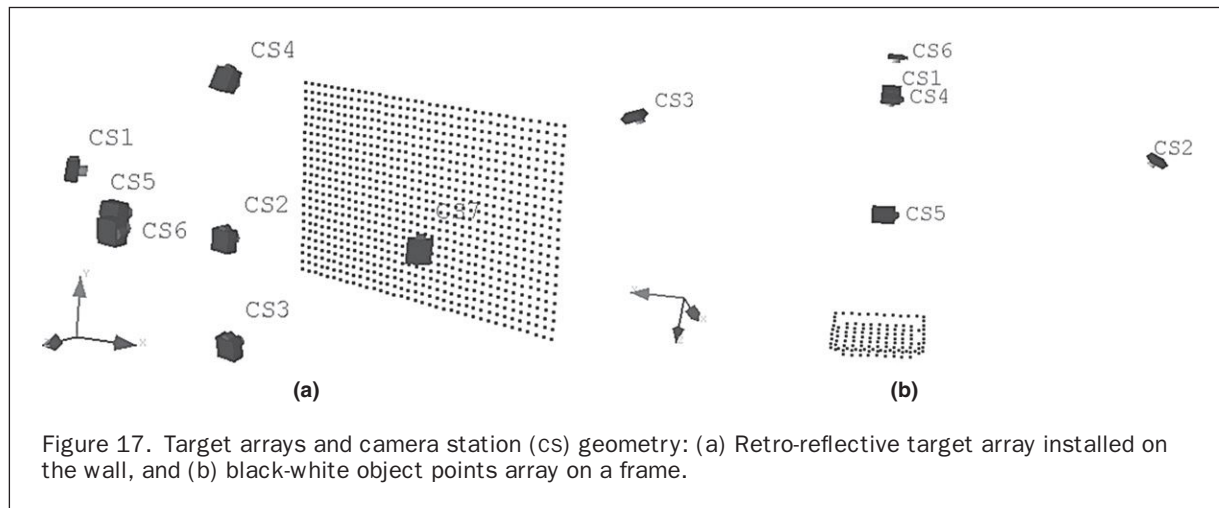
Figure 17. Target arrays and camera station (CS) geometry: (a) Retro-reflective target array installed on the wall, and (b) black-white object points array on a frame.

to test the polynomial models. Meanwhile, self-calibrations are also conducted with the same images to compare with the accuracy attained by the zoom/focus model developed in this paper. For the Edmund NT57-708 motorized zoom lens, only k_1 is employed, while for the other two lenses distortion parameters k_1, k_2, p_1, and p_2 are employed correspondingly in the self-calibration. The RMSE against true 3D coordinates pre-measured are recorded. As a consequence of different distances between target array and camera positions, accuracies are also normalized with the distances (Z_S). In addition, the accuracies of the calibration parameters from the proposed method are evaluated through independent check with self-calibration results. Moreover, to verify the necessity of involving focus settings in zoom lens model, the performance of the developed zoom/focus model is compared with the well-known Zoom-dependent model for the Edmund NT57-708 motorized zoom lens and the Canon EF 24 mm prime lens.

Self-Calibration versus Zoom/Focus Model
Shown in Table 6 is the summary of accuracies for the three lenses using self-calibration approach and the zoom/focus model developed in this paper. Prior to compare the outcome of the two approaches, it is meaningful to highlight some general aspects of the results. First and the most evident characteristic is that for the two zoom lenses (Edmund NT57-708 motorized zoom lens and Canon EF 28-105 mm

zoom lens), better accuracy can be anticipated at larger zoom settings for both self-calibration and zoom/focus model. Second, at relatively near focused distances (large focus settings), accuracies of zoom/focus model have deteriorated much compared with that of self-calibration. This is due to the severe influences of focus setting to principal distance which may be modeled less accurately. And third, for internal accuracy, the RMSE of image coordinate residuals, it is affected by both the accuracy of zoom/focus model and the image scale c/Z_S which will influence target extraction precision.

Turning to compare the outcome of different lenses, the accuracy of zoom/focus model attained by the Edmund NT57-708 motorized zoom lens surpasses the Canon EF 28-105 mm zoom lens, while similar accuracies are attained by self-calibration approach. The focus-dependent model for Canon EF 24 mm prime lens produces better outcome due to relatively small variation caused by focus compare to that caused by zoom.

As shown in Table 6, although the zoom/focus model show relatively lower accuracies compared with the results from the self-calibration method, the former is valuable for the previously mentioned close-range photogrammetric applications when performing a self-calibration is difficult or sometimes impossible. With the increasing interest of using off-the-shell zoom-lens cameras for various photogrammetric applications, the zoom/focus model is also valuable in

TABLE 6. RESULTS OF ZOOM/FOCUS MODEL COMPARED WITH SELF-CALIBRATION

Lens	Zoom Setting	Focus Setting	Zs (mm)	Self-Calibration		Zoom/Focus Model	
				RMSE of 3D Coordinates (mm)	RMSE of Image Residuals (pixels)	RMSE of 3D Coordinates (mm)	RMSE of Image Residuals (pixels)
Edmund NT57-708 motorized zoom lens	314 (18 mm)	615 (2 m)	2200	0.153 (1:14 000)	0.060	0.269 (1:8 100)	0.131
	388 (24 mm)	577 (4 m)	3700	0.189 (1:20 000)	0.089	0.326 (1:11 000)	0.155
	579 (50 mm)	348 (7 m)	6500	0.173 (1:37 000)	0.083	0.293 (1:22 000)	0.154
	620 (62 mm)	292 (9 m)	8300	0.192 (1:43 000)	0.061	0.330 (1:25 000)	0.143
Canon EF 28-105 mm zoom lens	75 mm	0.25 (4 m)	3500	0.158 (1:22 000)	0.133	0.285 (1:12 000)	0.181
	93 mm	0.45 (2.2 m)	2500	0.059 (1:42 000)	0.124	0.170 (1:15 000)	0.228
Canon EF 24 mm prime lens	24 mm	1.67 (0.6 m)	600	0.069 (1:9 000)	0.145	0.138 (1:5 000)	0.397
	24 mm	0 (infinite)	1500	0.155 (1:10 000)	0.068	0.190 (1:8 000)	0.082

offering better flexibility and feasibility in zoom lens calibration and modeling.

In addition, it is necessary to check the validity of the proposed zoom lens model directly by comparing the camera parameters with their true-values. As the true-values are unknown, the results from self-calibration method (considered to be the most accurate ones) are adopted instead. Shown in Figure 18 is the comparison of the camera parameters including the principal distance, principle point (x_0, y_0), radial distortion parameter k_1, and decentering distortion parameters p_1 and p_2, from the zoom/focus model and those from the self-calibration results for the same eight zoom/focus settings for the three cameras listed in Table 6.

It can be noted from Figure 18 that the principal distance and radial distortion parameter can be modeled fairly well. This is mainly because their behaviors are more regular than that of decentering distortions as illustrated in Figures 10 through 14. The principal points determined by the focus-of-expansion approach are proved to be very close to the results from the self-calibration method. As mentioned previously, the tiny ambiguities can be compensated by the EO parameters in the bundle block adjustment.

Zoom Dependent Model versus Zoom/Focus Model
Since focus will cause significant variation to intrinsic parameters as discussed above, accuracy loss can be anticipated if focus setting is intentionally elided in modeling zoom lens. To quantitatively evaluate the loss, two lenses are involved in the test, the Edmund NT57-708 motorized zoom lens and the Canon EF 24 mm prime lens. Focus setting is deliberately ignored by setting it to infinite to simulate the behavior of zoom-dependent model. The same images are used for both zoom-dependent and zoom/focus models.

Shown in Table 7 is the comparison between the two adopted models. The texts in bold format in the last four columns are the ones using zoom-dependent model. The others are the results from the zoom/focus model. As anticipated, eliding the effect of focus will cause dramatic accuracy loss, especially at close ranges. However around infinite focus, almost equivalent results can be attained. For example, for the zoom setting of 620 for the Edmund NT57-708 motorized zoom lens, the two focus settings (292 and 200) are close, and the derived accuracies are also close to each other.

Conclusions and Discussion

This paper has presented a flexible method for zoom lens calibration and modeling using a planar checkerboard. The following conclusions were reached based on the study including the experimental analyses:

1. Flexible and effective ways for zoom-lens calibration include fixing the principal point to an image point through the focus-of-expansion approach and using images of the checkerboard taken at varying object distances with varying rotations or roll angles to form convergent image geometry;
2. The strategy of using a scale parameter employed in this study proved able to model the influences of focus changes on principal distance and enable autofocus during zoom lens calibration process. Different functions should be used to model the scale parameters for different lenses since the tendency of variation is different and the order of polynomial is different. The focus settings impact the principal distance for all the three different adjustable lenses studied in this paper. Although this impact tends to be insignificant at small focal lengths and around focusing infinity, its impact increases with increasing focal length and decreasing focused distance;
3. Polynomials are simple and effective ways of modeling the calibration parameter variations in relation to the various zoom and focus settings. Through the methods developed in this study, relative accuracies ranging from 1:5 000 to 1:25 000 have been achieved for measurements using the three different lenses.

It should be noted that, in this proposed method the principal point is determined by a focus-of-expansion strategy, and the possible ambiguity in principle point can be compensated in the subsequent bundle adjustment as proved in the experimental analysis. While in some applications with direct orientation procedures when the bundle adjustment is not involved, the possible ambiguity in principle point might be magnified by the photogrammetric scale. A quantitative evaluation of this issue is beyond the scope of this paper.

Currently more off-the-shelf cameras which provide various zoom capabilities are commercially available. Development of a flexible approach for zoom-lens calibration that does not rely on a professional calibration field will significantly facilitate the use of zoom-lens cameras including the "off the shelf" zoom-lens cameras in various applications such as robotic exploration, hazard monitoring, traffic monitoring, and security surveillance.
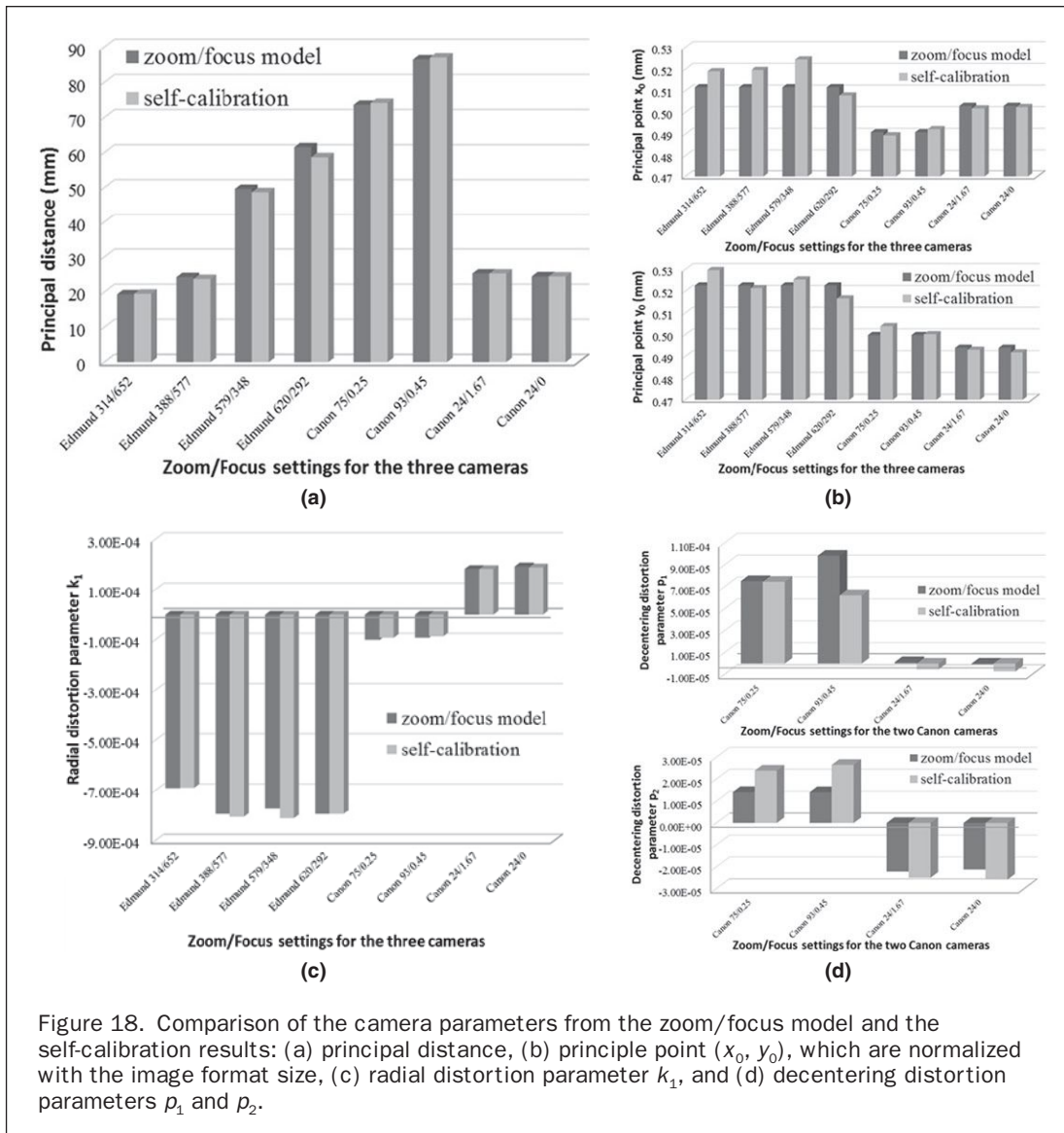
Figure 18. Comparison of the camera parameters from the zoom/focus model and the self-calibration results: (a) principal distance, (b) principle point (x_0, y_0), which are normalized with the image format size, (c) radial distortion parameter k_1, and (d) decentering distortion parameters p_1 and p_2.

TABLE 7. COMPARISON OF ZOOM-DEPENDENT MODEL AND ZOOM/FOCUS MODEL

Lens	Zoom Setting	Focus Setting	Zs (mm)	RMS of Image Residuals (pixels)	RMSE of 3D Coordinates (mm)
Edmund NT57–708 motorized zoom lens	314 (18 mm)	615 (2 m)	2200	0.1311	0.269 (1:8 100)
		200 (infinite)	**2200**	**0.4524**	**0.497 (1:4 400)**
	620 (62 mm)	292 (9 m)	8300	0.1430	0.330 (1:25 000)
		200 (infinite)	**8300**	**0.1676**	**0.357 (1:23 000)**
Canon EF 24 mm prime lens	24 mm	1.67 (0.6 m)	600	0.3970	0.139 (1:5 000)
		0 (infinite)	**600**	**5.0863**	**0.698 (1:700)**

References

Abraham, S., and T. Hau, 1997. Towards autonomous high precision calibration of digital cameras, *Proceedings of SPIE Videometrics V* (S.F. El-Hakim, editor), 3174: 82–93.

Ahmed, M.T., and A.A. Farag, 2000. A neural optimization framework for zoom lens camera calibration, *Proceedings of the IEEE 2000 Conference on Computer Vision and Pattern Recognition (CVPR 2000)*, Hilton Head Island, South Carolina, 13-15 June, Vol. 1, pp. 1403–1409.

Brauer-Burchardt, C., and K. Voss, 2001. A new algorithm to correct fish-eye-and strong wide-angle-lens-distortion from single images, *Proceedings of the International Conference on Image Processing*, Vol. 1, pp. 225–228.

Brown, D.C., 1971. Close-range camera calibration, *Photogrammetric Engineering*, 37(8):855–866.

Clarke, T.A., and J.G. Fryer, 1998. The development of camera calibration methods and models, *The Photogrammetric Record*, 16(91):51–66.

Clarke, T.A., X. Wang, and J.G. Fryer, 1998. The principal point and CCD cameras, *The Photogrammetric Record*, 16(92):293–312.

Ergun, B., 2010. Photogrammetric observing the variation of intrinsic parameters for zoom lenses, *Scientific Research and Essays*, 5(5):461–467.

Faig, W., 1975. Calibration of close-range photogrammetric systems: Mathematical formulation, *Photogrammetric Engineering & Remote Sensing*, 41(12):1479–1486.

Fryer, J.G., and D.C. Brown, 1986. Lens distortion for close-range photogrammetry, *Photogrammetric Engineering & Remote Sensing*, 52(1):51–58.

Fryer, J.G., 1996. Camera calibration, *Close-range Photogrammetry and Machine Vision* (K.B. Atkinson, editor), Whittles Publishing, pp. 156–179.

Fraser, C.S., 1997. Digital camera self-calibration, *ISPRS Journal of Photogrammetry and Remote Sensing*, 52(4):149–159.

Fraser, C.S., and S. Al-Ajlouni, 2006. Zoom-dependent camera calibration in digital close-range photogrammetry, *Photogrammetric Engineering & Remote Sensing*, 72(9):1017–1026.

Li, M., and J. Lavest, 1996. Some aspects of zoom lens camera calibration, *IEEE Transactions on Pattern Analysis and Machine Intelligence*, 18(11):1105–1110.

Malacara, D., and Z. Malacara, 1994. *Handbook of Lens Design*, Marcell Dekker, Inc., New York, 600 p.

Remondino, F., and C.S. Fraser, 2006. Digital camera calibration methods: Considerations and comparisons, *International Archives of the Photogrammetry, Remote Sensing and Spatial Information Sciences*, XXXVI(Part 5):266–272.

Sanz-Ablanedo, E., J.H. Chandler and R. Wackrow, 2012. Parameterising internal camera geometry with focusing distance, *The Photogrammetric Record*, 27(138):210–226.

Shih, S., Y. Hung, and W. Lin, 1996. Accuracy analysis on the estimation of camera parameters for active vision systems, *Proceedings of International Conference on Pattern Recognition*, Vienna, Austria, August.

Stamatopoulos, C., and C.S. Fraser, 2011. Calibration of long focal length cameras in close range photogrammetry, *The Photogrammetric Record*, 26(135):339–360.

Sturm, P., S. Ramalingam, J.P. Tardif, S. Gasparini, and J. Barreto, 2011. *Camera Models and Fundamental Concepts Used in Geometric Computer Vision (Foundations and Trends (R) in Computer Graphics and Vision)*, Now Publishers, Inc, 196 p.

Tarabanis, K., R. Tsai, and D. Goodman, 1994. Calibration of a computer controlled robotic vision sensor with a zoom lens, *CVGIP: Image Understanding*, 59(2):226–241.

Tsai, R., 1987. A versatile camera calibration technique for high-accuracy 3D machine vision metrology using off-the-shelf TV cameras and lenses, *IEEE Journal of Robotics and Automation*, 3(4):323–344.

Wang, Z.Z., 1990. *Principles of Photogrammetry [with Remote Sensing]*, Press of Wuhan Technical University of Surveying and Mapping, Publishing House of Surveying and Mapping, Beijing.

Wiley, A.G., and K.W. Wong, 1995. Geometric calibration of zoom lenses for computer vision metrology, *Photogrammetric Engineering & Remote Sensing*, 61(1):69–74.

Willson, R.G., 1994. *Modelling and Calibration of Automated Zoom Lenses*, PhD Dissertation, Robotics Institute, Carnegie Mellon University, Pittsburgh, Pennsylvania, 171 p.

Zhang, Z., 2000. A flexible new technique for camera calibration, *IEEE Transactions on Pattern Analysis and Machine Intelligence*, 22(11):1330–1334.